

Non-adiabatic transitions near avoided crossings: theory and numerics

R. Bourquin, V. Gradinaru and G.A. Hagedorn*

Research Report No. 2011-33
May 2011

Seminar für Angewandte Mathematik
Eidgenössische Technische Hochschule
CH-8092 Zürich
Switzerland

*Department of Mathematics and Center for Statistical Mechanics, Mathematical Physics, and Theoretical Chemistry, Virginia Polytechnic Institute and State University, Blacksburg, Virginia 240610123, USA

Non-Adiabatic Transitions near Avoided Crossings: Theory and Numerics

Raoul Bourquin,^a Vasile Gradinaru,^a George A. Hagedorn^b

April 8, 2011

Abstract

We present a review of rigorous mathematical results about non-adiabatic transitions in molecular systems that are associated with avoided crossings of electron energy level surfaces. We then present a novel numerical technique for studying these transitions that is based on expansions in semiclassical wavepackets.

1 Introduction

In the standard time-dependent Born-Oppenheimer approximation for molecular propagation, the electrons obey an adiabatic approximation. This approximation can break down at avoided crossings. Avoided crossings are nuclear configurations where electron energy levels approach close to one another. The resulting non-adiabatic dynamics plays an important role in physics, chemistry, and biology [19, 18, 17, 25].

Because of its importance in applications, the problem of simulating non-adiabatic dynamics in the presence of avoided crossings has been studied often. Probabilistic surface-hopping algorithms [23, 22, 16] are frequently used, since direct integration of the Schrödinger equation is considered too expensive, even with modern computers. One direct method, developed and used by the quantum chemistry community, is the Time-Dependent Discrete Variable Representation or TDDVR method [20]. A second method [4], based on semiclassical wavepackets, is a generalization of the TDDVR method and is expected to yield accurate results.

^aSeminar for Applied Mathematics ETH Zürich, CH-8092 Zürich, Switzerland

^bDepartment of Mathematics and Center for Statistical Mechanics, Mathematical Physics, and Theoretical Chemistry, Virginia Polytechnic Institute and State University, Blacksburg, Virginia 24061-0123, U.S.A.

The final publication is at <http://www.springerlink.com/index/4108L62372454J71.pdf>

In Section 2 of this paper, we review rigorous mathematical results on non-adiabatic transitions caused by avoided crossings when the nuclei have one degree of freedom. In Sections 3 and 4, we present the results of numerical simulations that use the semiclassical wavepacket approach.

2 Theoretical Results concerning Propagation through Avoided Crossings

As mentioned in the introduction, we shall restrict attention to situations in which the nuclei have just one degree of freedom. There are some other results [11] for avoided crossings with “small gaps” (as defined below) when the nuclei have more degrees of freedom.

There are only two situations for which mathematically rigorous results are known for propagation of molecular wave functions through generic avoided crossings in the Born–Oppenheimer limit. We describe both situations in this section. The first [11, 21] involves avoided crossings with small gaps, *i.e.*, avoided crossings whose gaps are $O(\epsilon^p)$ for p close to 1, where ϵ is the Born–Oppenheimer parameter. The second involves avoided crossings with small gaps that are fixed as ϵ is decreased. To describe these two situations, we begin with a definition of avoided crossings.

Definition Suppose $h(x, \delta)$ is a family of self-adjoint operators with a fixed domain \mathcal{D} in a Hilbert space \mathcal{H} for $x \in (x_1, x_2)$ and $\delta \in [0, \alpha)$. Suppose the resolvent of $h(x, \delta)$ is C^4 in both variables as an operator from \mathcal{D} to \mathcal{H} . Suppose $h(x, \delta)$ has two eigenvalues $E_{\mathcal{A}}(x, \delta)$ and $E_{\mathcal{B}}(x, \delta)$ that are isolated from the rest of the spectrum of $h(x, \delta)$. Assume further that there exists $x_0 \in (x_1, x_2)$, such that $x = x_0$ is the only solution to $E_{\mathcal{A}}(x, 0) = E_{\mathcal{B}}(x, 0)$, and that $E_{\mathcal{A}}(x, \delta) \neq E_{\mathcal{B}}(x, \delta)$ whenever $\delta > 0$. Then we say $h(x, \delta)$ has an avoided crossing at the point x_0 .

We restrict attention to the case where $E_{\mathcal{A}}$ and $E_{\mathcal{B}}$ are simple eigenvalues except when $x = x_0$ and $\delta = 0$. For convenience, we assume $x_0 = 0$, $x_1 = -\infty$, and $x_2 = \infty$. These are Type 1 avoided crossings in the classification given in [9]. By a proper choice of basis, the restriction $h(x, \delta)$ to the spectral subspace associated with $E_{\mathcal{A}}(x, \delta)$ and $E_{\mathcal{B}}(x, \delta)$ generically can be put in the normal form

$$h(x, \delta) = \begin{pmatrix} V(x, \delta) & 0 \\ 0 & V(x, \delta) \end{pmatrix} + \begin{pmatrix} b_1x + b_2\delta & c_2\delta \\ c_2\delta & -b_1x - b_2\delta \end{pmatrix} + \mathcal{O}(x^2 + \delta^2).$$

Thus, the two eigenvalues have the forms

$$E_{\mathcal{A}}(x, \delta) = V(x, \delta) + \sqrt{(b_1x + b_2\delta)^2 + c_2^2\delta^2} + \mathcal{O}(x^2 + \delta^2)$$

and

$$E_{\mathcal{B}}(x, \delta) = V(x, \delta) - \sqrt{(b_1x + b_2\delta)^2 + c_2^2\delta^2} + \mathcal{O}(x^2 + \delta^2).$$

The corresponding eigenvectors will be denoted by $v_{\mathcal{A}}$ and $v_{\mathcal{B}}$.

The Landau–Zener model [15, 24] is the special case with

$$h(x, \delta) = \begin{pmatrix} x & \delta \\ \delta & -x \end{pmatrix}.$$

The models used in chemistry usually involve exponential localization in space [22], so in the later sections of this paper, we consider the example of a related model that has the advantage that the potential term approaches its limits exponentially fast:

$$h(x, \delta) = \begin{pmatrix} \frac{1}{2} \tanh(x) & \frac{1}{2} \delta \\ \frac{1}{2} \delta & -\frac{1}{2} \tanh(x) \end{pmatrix} \quad (1)$$

$$\text{with eigenvalues } \pm \frac{1}{2} \sqrt{\delta^2 + \tanh(x)^2}.$$

See Figure 1. Since $\tanh(x) = x - \frac{1}{3}x^3 + \dots$ for $|x| < \frac{\pi}{2}$, this example fits into our setting with $V(x, \delta) = 0$, $b_1 = c_2 = \frac{1}{2}$, $b_2 = 0$ and the remainder $\mathcal{O}(x^3)$ independent of δ . We note that realistic molecules have Coulomb potentials which give rise to electronic Hamiltonians that do not satisfy the smoothness assumptions used here. However, these non-smooth potentials are accommodated with regularization techniques [7, 14].

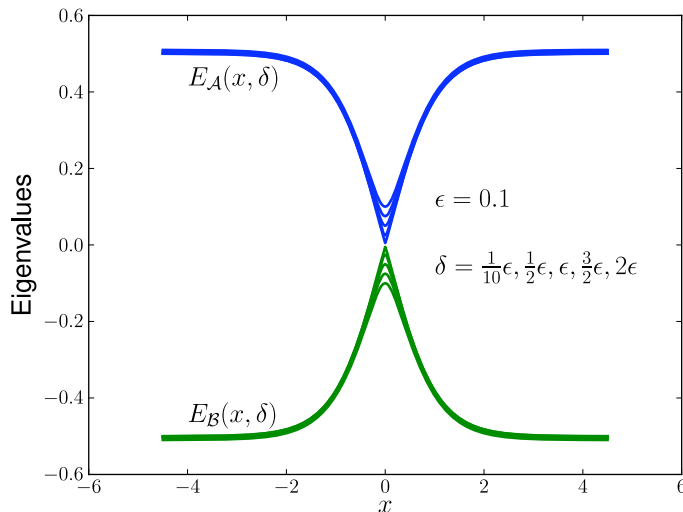


Figure 1: Electronic energy levels depending on gap parameter δ

The principal objects used in this paper are semiclassical wavepackets which in the one-dimensional case are parametrized Hermite functions. Given a set of parameters q, p, Q, P , a family of semiclassical wavepackets $\{\varphi_k^\epsilon[q, p, Q, P]\}$ is an orthonormal basis of $L^2(\mathbb{R})$ that is constructed in [10] from the Gaussian

$$\varphi_0^\epsilon[q, p, Q, P](x) = (\pi)^{-\frac{1}{4}} (\epsilon Q)^{-\frac{1}{2}} \exp\left(\frac{i}{2\epsilon^2} PQ^{-1}(x-q)^2 + \frac{i}{\epsilon^2} p(x-q)\right),$$

via a raising operator. In the notation used here, Q and P correspond to A and iB of [5, 6, 10], respectively. Note that Q and P must obey the compatibility condition $\overline{Q}P - \overline{P}Q = 2i$, see [10]. One can get an impression of the roles of the parameters ϵ, q, p, Q , and P in the one-dimensional case from Figure 2. Each state $\varphi_k(x) = \varphi_k^\epsilon[q, p, Q, P](x)$ is concentrated in position near q and in momentum near p with uncertainties $\epsilon|Q|\sqrt{k + \frac{1}{2}}$ and $\epsilon|P|\sqrt{k + \frac{1}{2}}$, respectively. The recurrence relation

$$Q\sqrt{k+1}\varphi_{k+1}^\epsilon(x) = \frac{\sqrt{2}}{\epsilon}(x-q)\varphi_k^\epsilon(x) - \overline{Q}\sqrt{k}\varphi_{k-1}^\epsilon(x) \quad (2)$$

permits us to compute the functions φ_k at any given value x .

In [11], molecular wave packets initially associated with one of the two energy levels are propagated through the avoided crossing with $\delta = \epsilon$, the

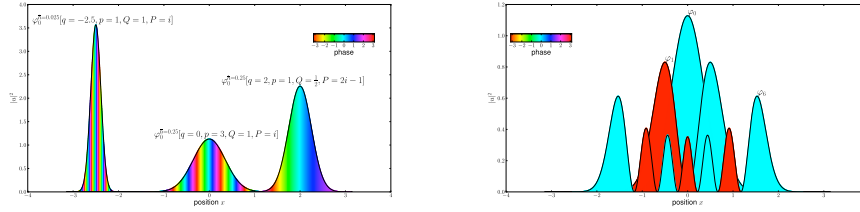


Figure 2: Left: first member of different families of semiclassical wavepackets. Right: a few members of the family with $q = 0$, $p = 0$, $Q = 1$, $P = i$

Born–Oppenheimer parameter. The Schrödinger equation for this situation is

$$i \epsilon^2 \frac{\partial \psi}{\partial t} = -\frac{\epsilon^4}{2} \frac{\partial^2 \psi}{\partial x^2} + h(x, \epsilon) \psi. \quad (3)$$

If the initial wave function is associated with $E_{\mathcal{A}}$, then the initial condition at some negative time $-T$ is taken to be

$$\psi(x, 0) = \varphi_l^\epsilon[q, p, Q, P](x) v_{\mathcal{A}}(x, \epsilon). \quad (4)$$

The results of [21] are closely related, but with $\delta = \epsilon^p$, with p close to 1. The cases $p < 1$, $p = 1$, and $p > 1$ display different results that we describe below.

The other situation in which there are rigorous results involves choosing a fixed, but sufficiently small value of $\delta > 0$, independent of ϵ . These results [12] describe a scattering situation for the Schrödinger equation

$$i \epsilon^2 \frac{\partial \psi}{\partial t} = -\frac{\epsilon^4}{2} \frac{\partial^2 \psi}{\partial x^2} + h(x, \delta) \psi. \quad (5)$$

In this case $E_{\mathcal{A}}$ and $E_{\mathcal{B}}$ and the corresponding eigenvectors are assumed to approach constants sufficiently rapidly as x approaches $\pm\infty$. If the incoming wave function was associated with $E_{\mathcal{A}}$ and incident from the left, then for large negative times t , $\psi(x, t)$ is assumed asymptotic to

$$e^{i(p_0^2/2 - E_{\mathcal{A}}(-\infty, \delta))t/\epsilon^2} \varphi_l^\epsilon[q_0 + p_0 t, p_0, Q_0 + P_0 t, P_0](x) v_{\mathcal{A}}(x, \delta), \quad (6)$$

with $p_0 > 0$.

2.1 Results for the Situation of a Small Critical Gap

The critical situation for small gaps is the one where the gap is proportional to ϵ . In this section we describe the results of [11] for Type 1 Avoided Crossings when the nuclear configuration parameter x is one-dimensional and δ is proportional to ϵ .

We choose the initial nuclear position and momentum q_0 and p_0 at some negative time so that the associated classical path determined by

$$\begin{aligned}\dot{q}^{\mathcal{C}}(t) &= p^{\mathcal{C}}(t) \\ \dot{p}^{\mathcal{C}}(t) &= -V'(q^{\mathcal{C}}(t), \epsilon)\end{aligned}$$

passes through the avoided crossing near time $t = 0$. By this we mean that we require

$$\begin{aligned}q^{\mathcal{C}}(0) &= 0 \\ p^{\mathcal{C}}(0) &= p^0 + \mathcal{O}(\epsilon),\end{aligned}$$

with $p^0 > 0$. The small ϵ asymptotics of the solutions to the initial value problems

$$\begin{aligned}\dot{q}^{\mathcal{A}}(t, \epsilon) &= p^{\mathcal{A}}(t, \epsilon) \\ \dot{p}^{\mathcal{A}}(t, \epsilon) &= -E'_{\mathcal{A}}(q^{\mathcal{A}}(t, \epsilon), \epsilon), \\ q^{\mathcal{A}}(0, \epsilon) &= 0, \\ p^{\mathcal{A}}(0, \epsilon) &= p^0 + \mathcal{O}(\epsilon)\end{aligned}$$

and

$$\begin{aligned}\dot{q}^{\mathcal{B}}(t, \epsilon) &= p^{\mathcal{B}}(t, \epsilon) \\ \dot{p}^{\mathcal{B}}(t, \epsilon) &= -E'_{\mathcal{B}}(q^{\mathcal{B}}(t, \epsilon), \epsilon), \\ q^{\mathcal{B}}(0, \epsilon) &= 0, \\ p^{\mathcal{B}}(0, \epsilon) &= p^0 + \mathcal{O}(\epsilon)\end{aligned}$$

are determined in Section 2 of [11] up to $\mathcal{O}(|t^3| + \epsilon t^2)$ errors for the positions and up to $\mathcal{O}(t^2 + \epsilon|t|)$ errors for the momenta. These asymptotics are very complicated and contain various logarithmic terms. Analogous small t and

ϵ asymptotics are determined for the initial value problems

$$\begin{aligned}\dot{Q}^{\mathcal{A}}(t, \epsilon) &= P^{\mathcal{A}}(t, \epsilon), \\ \dot{P}^{\mathcal{A}}(t, \epsilon) &= -E''_{\mathcal{A}}(q^{\mathcal{A}}(t, \epsilon), \epsilon) Q^{\mathcal{A}}(t, \epsilon), \\ Q^{\mathcal{A}}(0, \epsilon) &= Q^0, \\ P^{\mathcal{A}}(0, \epsilon) &= P^0,\end{aligned}$$

and

$$\begin{aligned}\dot{Q}^{\mathcal{B}}(t, \epsilon) &= P^{\mathcal{B}}(t, \epsilon), \\ \dot{P}^{\mathcal{B}}(t, \epsilon) &= -E''_{\mathcal{B}}(q^{\mathcal{B}}(t, \epsilon), \epsilon) Q^{\mathcal{B}}(t, \epsilon), \\ Q^{\mathcal{B}}(0, \epsilon) &= Q^0, \\ P^{\mathcal{B}}(0, \epsilon) &= P^0.\end{aligned}$$

Small ϵ asymptotics for the classical action integrals $S^{\mathcal{A}}(t, \epsilon)$ and $S^{\mathcal{B}}(t, \epsilon)$ associated with these orbits are also determined.

The results of [11] are now obtained by an asymptotic matching procedure. For times $-T < t < -\epsilon^{1-\xi}$ there is an “incoming outer solution” to (3) with initial condition (4) that satisfies

$$\begin{aligned}\psi(t, \epsilon) &= F(|x - q^{\mathcal{A}}(t, \epsilon)|/\epsilon^{1-\delta'}) e^{iS^{\mathcal{A}}(t, \epsilon)/\epsilon^2} v_{\mathcal{A}}(x, \epsilon) \\ &\quad \times \varphi_l^\epsilon[q^{\mathcal{A}}(t, \epsilon), p^{\mathcal{A}}(t, \epsilon), Q^{\mathcal{A}}(t, \epsilon), P^{\mathcal{A}}(t, \epsilon)](x) \\ &\quad + \mathcal{O}(\epsilon^\xi).\end{aligned}$$

Here the uninteresting factor $F(\cdot)$ is a cut off function that must be inserted for technical reasons. The semiclassical wave packet φ_l is only large where $F(\cdot)$ takes the value 1. The error term is measured in the L^2 norm in x .

This incoming solution is then matched to an “inner solution” that involves parabolic cylinder functions of complex order and complex argument. For times $-\epsilon^{1-\xi'} \leq t \leq \epsilon^{1-\xi'}$ this inner solution agrees with an exact solution to (3) up to $\mathcal{O}(\epsilon^{1-3\xi'})$ errors. In the overlap region $-\epsilon^{1-\xi'} < t < -\epsilon^{1-\xi}$, the incoming outer solution and inner solution agree up to $\mathcal{O}(\epsilon^p)$ errors, where $p > 0$.

The inner solution is then matched to an “outgoing outer solution” that is a superposition of two standard Born–Oppenheimer approximate solu-

tions. For $\epsilon^{1-\xi} < t < T$, this outgoing outer solution is

$$\begin{aligned} \psi(t, \epsilon) &= C_{\mathcal{A}} F(|x - q^{\mathcal{A}}(t, \epsilon)|/\epsilon^{1-\delta'}) e^{iS^{\mathcal{A}}(t, \epsilon)/\epsilon^2} v_{\mathcal{A}}(x, \epsilon) \\ &\quad \times \varphi_l^\epsilon[q^{\mathcal{A}}(t, \epsilon), p^{\mathcal{A}}(t, \epsilon), Q^{\mathcal{A}}(t, \epsilon), P^{\mathcal{A}}(t, \epsilon)](x) \\ &+ C_{\mathcal{B}} F(|x - q^{\mathcal{B}}(t, \epsilon)|/\epsilon^{1-\delta'}) e^{iS^{\mathcal{B}}(t, \epsilon)/\epsilon^2} v_{\mathcal{B}}(x, \epsilon) \\ &\quad \times \varphi_l^\epsilon[q^{\mathcal{B}}(t, \epsilon), p^{\mathcal{B}}(t, \epsilon), Q^{\mathcal{B}}(t, \epsilon), P^{\mathcal{B}}(t, \epsilon)](x) \\ &+ \mathcal{O}(\epsilon^\xi). \end{aligned}$$

The values of $C_{\mathcal{A}}$ and $C_{\mathcal{B}}$ are determined by the Landau–Zener formula. In particular, we have the leading order transition probabilities

$$|C_{\mathcal{A}}|^2 = 1 - e^{-\frac{\pi c_2^4}{b_1^2 p^0}} \quad (7)$$

and

$$|C_{\mathcal{B}}|^2 = e^{-\frac{\pi c_2^4}{b_1^2 p^0}}. \quad (8)$$

This analysis is extremely tedious, but yields a rigorous proof of the leading order behavior of the full wave function.

We now make three observations about the results:

- 1.** A properly interpreted Landau–Zener formula based on the classical mechanics of the nuclei gives the correct leading order transition probabilities.
- 2.** We see that if the initial nuclear wave function is a φ_l , then the final full wave function is a superposition of two Born–Oppenheimer states in which the nuclear wave functions are both φ_l wavepackets that propagate independently according to the dynamics of the $E_{\mathcal{A}}$ and $E_{\mathcal{B}}$ levels.
- 3.** Conservation of the classical energy determines the classical orbit after the transition. At time zero, $p^{\mathcal{A}}(0, \epsilon) = p^0 + \mathcal{O}(\epsilon)$ and $p^{\mathcal{B}}(0, \epsilon) = p^0 + \mathcal{O}(\epsilon)$. The $\mathcal{O}(\epsilon)$ terms here are different, but are determined to leading order by conservation of the classical energy. Since the two effective potentials differ by an $\mathcal{O}(\epsilon)$ amount at the avoided crossing, the momenta also differ by an $\mathcal{O}(\epsilon)$ amount so that the energies are the same.

For the situation we describe in the section 2.3, none of these three observations will be valid. All three depend on the choice $\delta = \epsilon$ we have assumed throughout this section.

2.2 Results for the Situation with a Small, Non-critical Gap

The results of [21] are closely related to those of the previous section, except that the gap parameter δ can be $\mathcal{O}(\epsilon^p)$ for p in a neighborhood of 1.

When $p > 1$, δ/ϵ tends to zero, so the gap is smaller than in the previous section. Intuitively, this would be like having c_2 tend to zero in (7) and (8). Thus, one would expect $|C_{\mathcal{A}}|$ to tend to zero and $|C_{\mathcal{B}}|$ to tend to 1.

In contrast, when $p < 1$, δ/ϵ tends to infinity, and the gap is much larger. Again, one would be like having c_2 very large in (7) and (8). So, one would expect $|C_{\mathcal{A}}|$ to tend to 1 and $|C_{\mathcal{B}}|$ to tend to zero.

This is precisely what is proved in [21]. When δ/ϵ tends to zero, the system behaves as though it has an actual crossing [8], and the system makes the transition from the upper level to the lower level or *vice versa* to leading order. When δ/ϵ tends to infinity, the gap is large enough that to leading order, there is no transition, and the system stays on the same level. Furthermore, one sees that the three remarks at the end of section 2.1 still apply.

These results are again proved by asymptotic matching. They show that the case considered in the previous section is critical, and that slightly larger or slightly smaller gaps completely change the outcome as the system propagates through an avoided crossing.

2.3 Results for the Situation with a Fixed Gap

We now consider the situation described in [12], where $\delta > 0$ is small, but fixed, independent of ϵ . We assume that $h(x, \delta)$ is simply a 2×2 matrix. We further assume it is defined and analytic in the complex strip $\{x : |\text{Im } x| < \alpha\}$ and that $h(x, \delta)$ approaches limiting values $h(\pm\infty, \delta)$ sufficiently rapidly as the real part of x tends to $\pm\infty$, uniformly in a strip. We only consider wave functions whose total molecular energy is strictly above the suprema of both eigenvalues of $h(x, \delta)$ for all real x .

We assume $h(x, \delta)$ has exactly one avoided crossing, and that it has the generic form described above. In this case, the time-dependent Born-Oppenheimer approximation is exponentially accurate in $1/\epsilon^2$, uniformly in time. Thus, the probability of a non-adiabatic transition from one electronic level to the other, is bounded by $\exp(-\Gamma/\epsilon^2)$ for some $\Gamma > 0$. Thus, it is too small to be determined by any straightforward perturbation theory argument.

The strategy used in [12] is to expand the wave function at each time in

terms of the generalized eigenvectors of the full Hamiltonian

$$H(\epsilon, \delta) = -\frac{\epsilon^4}{2} \frac{\partial^2}{\partial x^2} + h(x, \delta).$$

These are solutions to the system of ordinary differential equations

$$H(\epsilon, \delta) \phi = E \phi.$$

When E is strictly above the suprema of both eigenvalues of $h(x, \delta)$, there are four independent solutions that intuitively correspond to left or right motion governed by the effective potentials $E_{\mathcal{A}}$ or $E_{\mathcal{B}}$. For small ϵ , one can establish a WKB approximation for each of these solutions that is valid for x in the complex strip. When δ is sufficiently small, the avoided crossing for real x is associated with a pair of complex conjugate crossings of the eigenvalues where $E_{\mathcal{A}}(x, \delta) = E_{\mathcal{B}}(x, \delta)$. This is one reason we assume $\delta > 0$ is sufficiently small. When one starts on the real x -axis, moves around such a generic crossing in the complex plane exactly once, and moves back to the real axis, the levels $E_{\mathcal{A}}$ and $E_{\mathcal{B}}$ are interchanged. As a result, one can analyze the transition by using the complex WKB approximation.

There are several exponentially small components one should expect for large times. The nuclei could reverse direction while the electrons stay in the initial level or switch levels. It is proved in [12] that the probability of this happening is exponentially smaller than the probability of making a non-adiabatic transition with the nuclei continuing to move in the same direction. This result depends on the total energy being above the suprema of both levels and $\delta > 0$ being small.

To keep the total energy strictly above both levels, one cannot simply use the φ_l for the nuclear wave functions; a momentum cut off must be inserted. In this discussion we shall suppress mentioning this technicality. However, for small enough ϵ , multiplying by the cut off only changes φ_l by an exponentially smaller amount than the errors we discuss here.

We now fix l and consider the solution to equation (5) with large negative t asymptotics given by (6). Since the time-dependent Born–Oppenheimer approximation is exponentially accurate, the main component of the full wave function stays associated with the $E_{\mathcal{A}}$ level for all times. We write the solution as a superposition of generalized eigenvectors of $H(\epsilon, \delta)$ and employ the complex WKB approximation. The piece of the full wave function that makes a non-adiabatic transition is thus written as an integral (because of the superposition). The large time and small ϵ asymptotics of this integral can be obtained by a rigorous version of Laplace’s technique. One obtains the following for the leading order behavior:

For sufficiently small ϵ the largest exponentially small correction to the Born–Oppenheimer propagation is the component that has made a non-adiabatic transition with the nuclear momentum with the same sign as the initial nuclear momentum. It has leading order large positive time asymptotics

$$C_l \epsilon^{-l} e^{-\gamma/\epsilon^2} e^{i((p^{\mathcal{B}})^2/2 - E_{\mathcal{B}}(\infty, \delta))t/\epsilon^2} \\ \times \varphi_0^\epsilon[q^{\mathcal{B}} + p^{\mathcal{B}}t, p^{\mathcal{B}}, Q^{\mathcal{B}} + P^{\mathcal{B}}t, P^{\mathcal{B}}](x) v_{\mathcal{B}}(x, \delta).$$

There are three surprising differences from the result in the previous section:

1. When $l = 0$, the magnitude $|C_0 e^{-\gamma/\epsilon^2}|$ is strictly greater than what one would obtain by using the Landau–Zener formula for the electron Hamiltonian with the classical position $q^{\mathcal{A}}(t, \delta)$ in place of x .
2. The classical energy $(p^{\mathcal{B}})^2/2 + E_{\mathcal{B}}(\infty, \delta)$ is strictly greater than the initial classical energy $p_0^2/2 + E_{\mathcal{A}}(-\infty, \delta)$ of (6).
3. For sufficiently small ϵ (that depends on l), one always obtains a φ_0 for the nuclear wavepacket after the transition, independent of the choice of l . Note, however, that the choice of l shows up in the factor ϵ^{-l} , so there is a strong dependence on l .

The reasons for these three observations become clear from the proof. For each generalized eigenfunction of the full Hamiltonian, the Landau–Zener formula gives the correct transition amplitude. That transition amplitude increases exponentially rapidly as the momentum is increased. When one makes the superposition of these generalized eigenfunctions, the higher momentum components are much more likely to make a non-adiabatic transition. This bias toward higher momenta causes the wave function after the transition to have energy greater than the average energy of the incident wave function. It is also responsible for the Landau–Zener formula based on the average momentum giving too small a transition amplitude. Finally, this extra shift in momentum occurs in the Gaussian part of the nuclear wavepacket. There is no corresponding shift of the Hermite polynomial in nuclear momentum space. So, the mean momentum of the Gaussian is strictly greater than the momenta where the Hermite polynomial has its zeros. Away from where the polynomial has its zeros, the polynomial behaves like its highest order term, which due to the scaling in ϵ looks like $\epsilon^{-l} p^l$. This is how the factor of ϵ^{-l} arises, and $p^l e^{-\kappa(p-p_0)^2/(2\epsilon)}$ is asymptotically a Gaussian if $p_0 \neq 0$. Thus, we obtain a φ_0 in this case instead of a φ_l .

This technique of proof is mathematically appealing, but it is not practical. It relies on the analytic continuations of the levels E_A and E_B , and the final quantities depend on solutions to equations that use those analytic continuations. For that reason, we have sought a reliable, stable numerical technique that can be used in applications when ϵ is small. The remainder of this paper is dedicated to developing such a technique.

3 Practical Propagation

In this section and the next, we present a new technique for the numerical propagation of molecular wave packets through avoided crossings. There are other techniques, and all of the techniques have various difficulties if ϵ is very small.

The numerical results presented in [11] and [13] were obtained by a Strang splitting and fast Fourier transform technique applied to the finite difference approximation to the Hamiltonian. This technique is limited to small spatial dimensions, and one must store the wave function at a huge number of points if ϵ is small.

Recently, a numerical technique [1, 2] has been developed that is motivated by optimal truncation of the time-dependent Born–Oppenheimer expansion. The Born–Oppenheimer expansion concentrates on a single electron energy surface, and it is asymptotic, but not convergent. The idea of optimal truncation is to take the expansion to the order that minimizes the error for any given ϵ . The central idea of [1] and [2] is to study non-adiabatic transitions between the optimally truncated wave functions. This “superadiabatic” approach is successful as long as ϵ is not too small, since the optimal number of terms in the Born–Oppenheimer expansion behaves like C/ϵ^2 . Also, the numerical results of [1, 2] appear to be very good for values of ϵ that are not too small, but are not consistent with the rigorous results of [12] in the $\epsilon \rightarrow 0$ limit.

We now present our new numerical algorithm. In the case of a well-separated energy level (*i.e.*, in the adiabatic Born–Oppenheimer model), the wave function is well approximated by a family of semiclassical wavepackets, whose dynamics is driven by the Schrödinger equation on that energy level [3, 4]. When the wave function ψ has several components and well-separated levels, the dynamics on each level can be approximated with a distinct family of semiclassical wavepackets. As long as the energy levels are far from each

other, there is little interaction between them, so each energy surface should dictate the dynamics of its own wave function. The interaction is non-trivial near an avoided crossing. In order to investigate this interesting case, we choose incoming initial conditions in terms of semiclassical wavepackets associated only with one energy level λ (it can be E_A or E_B). The wavepacket will be driven initially by its own energy level, *i.e.*, $\lambda(x)$ plays the role of the potential in this adiabatic Born-Oppenheimer case. In our propagation scheme (Algorithm 1) we keep $\lambda(x)$ as the guiding potential and use only its family of semiclassical wavepackets. The orthogonality between the members of one family of wavepackets simplifies the propagation.

We split $\lambda(x)$ into a local quadratic part u_0 and a non-quadratic remainder w_0 . This is done via a simple Taylor series expansion up to second order around q .

$$\begin{aligned} u_0(x) &= \lambda(q) + \lambda'(q)(x - q) + \frac{1}{2}\lambda''(q)(x - q)^2 \\ w_0(x) &= \lambda(x) - u_0(x). \end{aligned} \tag{9}$$

We can now write $h(\cdot, \delta)$ as a pure quadratic diagonal part U plus a non-quadratic remainder matrix W :

$$h = \begin{pmatrix} u_0 & 0 \\ 0 & u_0 \end{pmatrix} + \begin{pmatrix} h_{00} - u_0 & h_{01} \\ h_{10} & h_{11} - u_0 \end{pmatrix} = U + W. \tag{10}$$

The propagation of the wavepackets

$$\psi = \begin{pmatrix} 1 \\ 0 \end{pmatrix} \sum_{k=0}^{K-1} c_k^0 \varphi_k^\epsilon[q, p, Q, P] + \begin{pmatrix} 0 \\ 1 \end{pmatrix} \sum_{k=0}^{K-1} c_k^1 \varphi_k^\epsilon[q, p, Q, P]$$

is exact for the terms involving only the kinetic energy operator and the quadratic part of the potential energy operator. The coefficients of the wavepackets do not change under the influence of these operators, but they do under the action of the non-quadratic part W . The propagation scheme developed in [3] can now be used, at least until the system enters the non-adiabatic region, and even longer if we can afford to use enough basis functions. The evolution of the parameters q, p, Q, P is dictated by the quadratic part u_0 of the chosen guiding energy level λ . As in the tunneling problem [4], the orthogonal basis formed by the members of a single family of wavepackets might not be very well suited for the second component after passing the non-adiabatic region, but they still are a basis of L^2 and the propagation can be done.

Algorithm 1 Propagation of a vector-valued wavepacket

Require: A wavepacket at time t_j and a guiding energy level λ

// Propagate with the kinetic operator

$$q^{(j+\frac{1}{2})} := q^{(j)} + \frac{\tau}{2}p^{(j)}$$

$$Q^{(j+\frac{1}{2})} := Q^{(j)} + \frac{\tau}{2}P^{(j)}$$

$$S^{(j+\frac{1}{2},-)} := S^{(j)} + \frac{\tau}{4}p^{(j)}p^{(j)}$$

// Propagate with the local quadratic potential

$$p^{(j+1)} := p^{(j)} - \tau \nabla \lambda(q^{(j+1/2)})$$

$$P^{(j+1)} := P^{(j)} - \tau \nabla^2 \lambda(q^{(j+1/2)})Q^{(j+1/2)}$$

$$S^{(j+1/2,+)} := S^{(j+1/2,-)} - \tau \lambda(q^{(j+1/2)})$$

// Propagate with the non-quadratic remainder

$$C^{(j+1)} := \exp\left(-\tau \frac{i}{\epsilon^2} \mathbf{F}^{(j+1/2)}\right) C^{(j)}$$

// Propagate with the kinetic operator again

$$q^{(j+1)} := q^{(j+1/2)} + \frac{\tau}{2}p^{(j+1)}$$

$$Q^{(j+1)} := Q^{(j+1/2)} + \frac{\tau}{2}P^{(j+1)}$$

$$S^{(j+1)} := S^{(j+1/2,+)} + \frac{\tau}{4}p^{(j+1)}p^{(j+1)}$$

Return the wavepacket at time $t_{j+1} = t_j + \tau$

How should one compute the Galerkin matrix \mathbf{F} for the non-quadratic remainder? Since we have considered only two energy levels, we have two vectors with K complex coefficients each, corresponding to the approximations of each part of the wave function ψ . We stack these vectors in a long block vector C :

$$C := \left(c_0^0, \dots, c_{K-1}^0 \mid c_0^1, \dots, c_{K-1}^1 \right)^T. \quad (11)$$

Note that the case of L energy levels yields a vector with LK complex entries. The matrix \mathbf{F} will be of size $LK \times LK$ and will consist of blocks $F_{i,j}$ of size $K \times K$. Attention is now required: $W(x)$ is a matrix, thus each block $F_{i,j}$ is given by $\int_{\mathbb{R}} \tilde{F}_{i,j}(x) dx$, where

$$\tilde{F}_{i,j}(x) := W_{i,j}(x) \begin{pmatrix} \vdots \\ \dots & \overline{\varphi_k(x)}\varphi_l(x) & \dots \\ \vdots \end{pmatrix}, \quad (12)$$

and hence the methods presented in [3] can be applied for the elements of W . In Algorithm 2 we make use of appropriate quadrature points γ and weights ω .

Algorithm 2 Building the block matrix \mathbf{F} for propagation

Require: A wavepacket (one family on L states)**Require:** W a $L \times L$ matrix of scalar functions// Initialize \mathbf{F} as the zero-matrix $\mathbf{F} \in \mathbb{R}^{LK \times LK}, \quad \mathbf{F} := \mathbf{0}$ // Evaluate the functions in the family for all quadrature nodes γ $B := (\beta_0, \dots, \beta_{K-1})$

// Iterate over all row and column blocks of this matrix

for $i = 0$ **to** $L - 1$ **do** **for** $j = 0$ **to** $L - 1$ **do** // Evaluate the function $W_{i,j}$ for all quadrature nodes γ $(v_0, \dots, v_{N-1}) := (W_{i,j}(\gamma_0), \dots, W_{i,j}(\gamma_{N-1}))$

// Set up a zero matrix for the local block

 $F \in \mathbb{R}^{K \times K}, \quad F := \mathbf{0}$ // Iterate over all pairs of quadrature points and weights (γ_l, ω_l) **for** $l = 0$ **to** $N - 1$ **do** $F := F + v_l \epsilon \cdot B^H B \cdot \omega_l$ **end for** // Insert the block F into the block matrix \mathbf{F} $\mathbf{F}_{i,j} := F$ **end for****end for****return** \mathbf{F}

The same algorithm can be used for the transformation from the canonical basis to the eigenbasis by simply replacing W by the matrix M that diagonalizes the potential matrix h . This transformation is used in order to compute observables related to each state; the wave function is written as the sum of its adiabatic components, *e.g.*, in case of two energy levels given by the eigenvectors $v_{\mathcal{A}}$ and $v_{\mathcal{B}}$:

$$\psi(x, t) = \Phi_{\mathcal{A}}(x, t) + \Phi_{\mathcal{B}}(x, t) = \phi_{\mathcal{A}}(x, t)v_{\mathcal{A}}(x) + \phi_{\mathcal{B}}(x, t)v_{\mathcal{B}}(x).$$

4 Numerical Results

In this section we present results from the propagation method in various situations. In the case of a single avoided crossing, the semiclassical wavepackets reproduce the numerical results presented in [11] and [13]. Those results were obtained with Strang splitting and Fourier transformation and were consistent with the theoretical predictions.

We now consider the time-dependent Schrödinger equation (3) with the matrix potential (1). While the theoretical investigations consider the asymptotics as $\epsilon \rightarrow 0$, concrete chemical systems have a given fixed ϵ . We focus now on the case $\epsilon = 0.2$ when the solution based on the Fourier transformation and Strang splitting can serve as a reference solution since it is still feasible and accurate. Our main interest is to see whether we may rely on the propagation of the semiclassical wavepackets for various sizes of the gap δ . The initial value is taken to be the eigenvector associated with the upper energy level times the semiclassical wavepacket φ_2 with parameters $q = -6$, $p = 1$, $Q = 1 - 6i$, $P = i$. Usually, the simpler case of the Gaussian φ_0 as initial value is considered, but φ_2 allows us better to illustrate the capability of our method to reproduce the sophisticated quantum phenomena that occur when the gap δ is large. We performed the propagation with the time-step $\tau = 0.02$ from time 0 until the end-time $T = 10$, separately for several values of the gap δ . Figure 3 shows the position space plot at times $t = 5$ and $t = 10$ of the probability density for being on the upper energy level $\lambda_0 = E_{\mathcal{A}}(\cdot, \delta)$ and on the lower energy level $\lambda_1 = E_{\mathcal{B}}(\cdot, \delta)$ for $\delta = \epsilon$. We notice that after the complicated behavior near the avoided crossing, the outgoing wave function on the lower energy level far from the avoided crossing has the shape of a semiclassical wavepacket φ_2 moving faster than the component on the upper level.

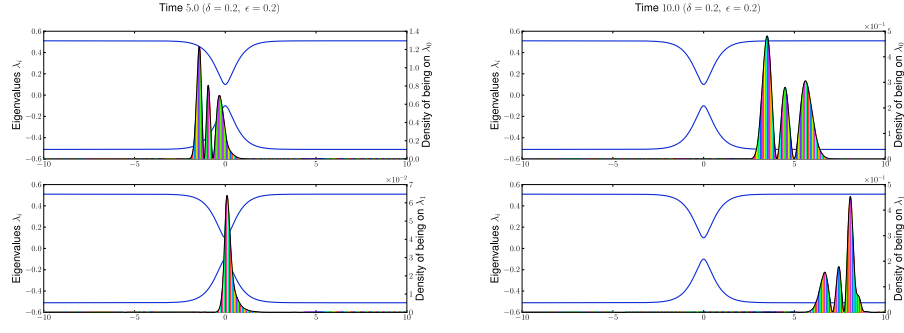


Figure 3: Position space plot at time $t = 5$ (left) and $t = 10$ (right) of the probability density of being on the upper energy level $\lambda_0 = E_{\mathcal{A}}(\cdot, \delta)$ and on the lower energy level $\lambda_1 = E_{\mathcal{B}}(\cdot, \delta)$ in the case $\delta = \epsilon = 0.2$. The left scale refers to the energy levels, while the right scale refers to the squared absolute values of the components $\Phi_{\mathcal{A}}$ (upper) and $\Phi_{\mathcal{B}}$ (lower) on the two levels.

In contrast, when $\delta = 5\epsilon$, the leading term of the outgoing wave function on the lower energy level far from the avoided crossing is a very small Gaussian φ_0 , while near the avoided crossing the transmitted part is much larger. See Figure 4. The size and the shape of the outgoing wave function on the lower energy level changes dramatically, as it moves away from the critical region, as we can see in Figure 5. Note the different magnitudes! The maximum squared absolute value of the component $\Phi_{\mathcal{B}}$ is nearly $1.8 \cdot 10^{-4}$ at time $t = 5$ (lower-left part of Figure 4), and nearly $4.2 \cdot 10^{-6}$ at time $t = 7.4$ (Figure 5). At the time $t = 9$, we clearly see two components on the lower level (Figure 5): The first has its maximum squared absolute value nearly $1.3 \cdot 10^{-8}$, while the second is slightly lower and wider and is located near a larger value of x . This latter component dominates at all later times, and we see it (lower-right part of Figure 4) at $t = 10$ having its maximum squared absolute value at about $6.5 \cdot 10^{-9}$.

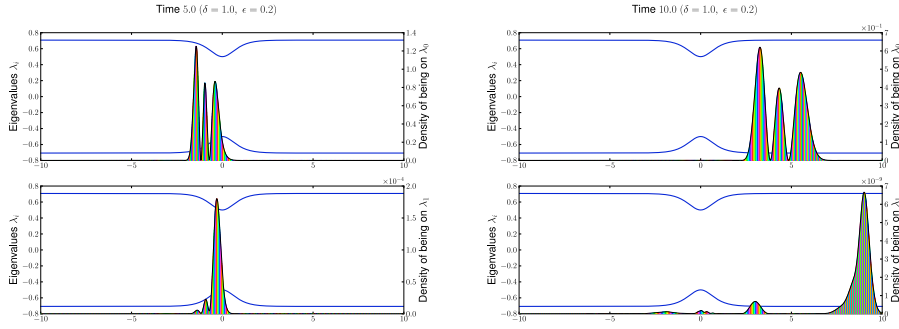


Figure 4: Position space plot at time $t = 5$ (left) and $t = 10$ (right) of the probability density of being on the upper energy level $\lambda_0 = E_{\mathcal{A}}(\cdot, \delta)$ and on the lower energy level $\lambda_1 = E_{\mathcal{B}}(\cdot, \delta)$ in the case $\delta = 5\epsilon = 1$. The left scale refers to the energy levels, while the right scale refers to the squared absolute values of the components $\Phi_{\mathcal{A}}$ (upper) and $\Phi_{\mathcal{B}}$ (lower) on the two levels. Note the different magnitudes!

The probability density for transition to the lower level $\lambda_1 = E_{\mathcal{B}}(\cdot, \delta)$ as well as the probability density for remaining in the excited state $\lambda_0 = E_{\mathcal{A}}(\cdot, \delta)$ for various gap sizes δ are plotted in Figures 6 and 7. At a gap $\delta \approx \epsilon$ the two components of the wave function $\Phi_{\mathcal{A}}$ and $\Phi_{\mathcal{B}}$ are roughly the same size. Much less (but still of the shape of a φ_2 , not shown in a picture here) is transmitted to the lower level for $\delta = 2\epsilon$, while the exponentially small transition is reproduced correctly by our numerical method for $\delta = 5\epsilon$. The

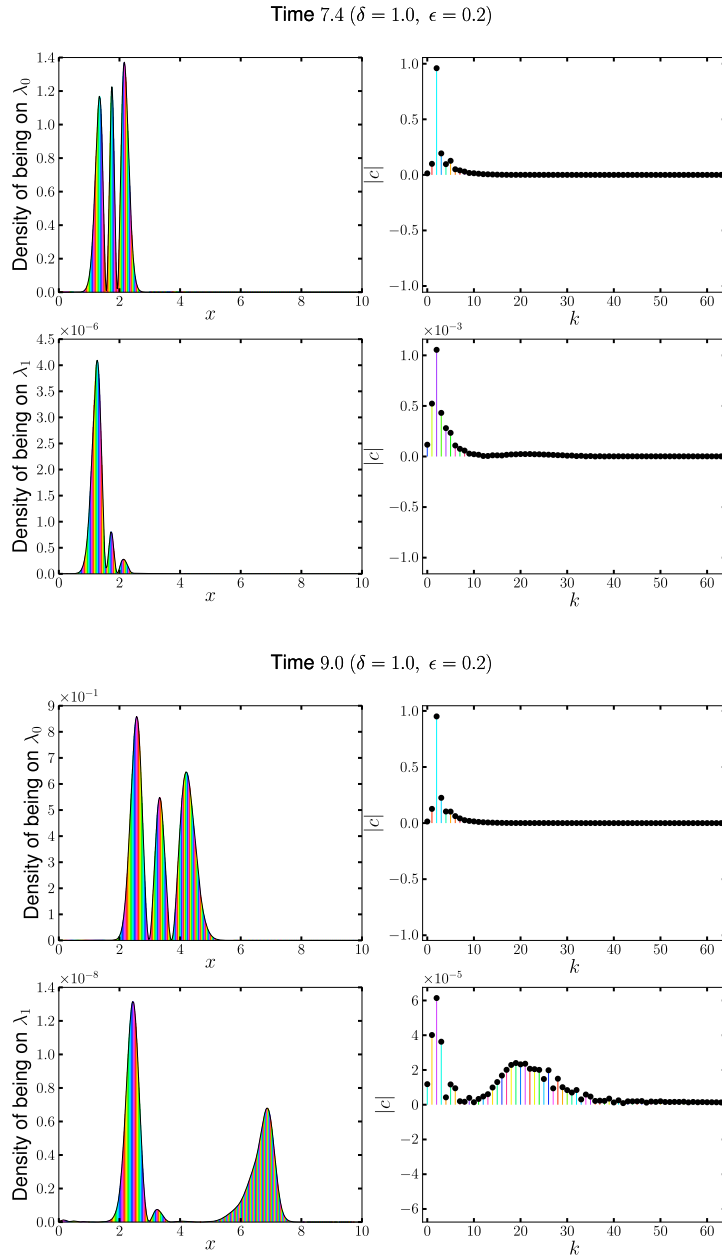


Figure 5: Probability density of being on each of the two levels (left) and the absolute values of the semiclassical coefficients c_k (right) in the case $\delta = 5\epsilon = 1$ at times $t = 7.9$ and $t = 9$.

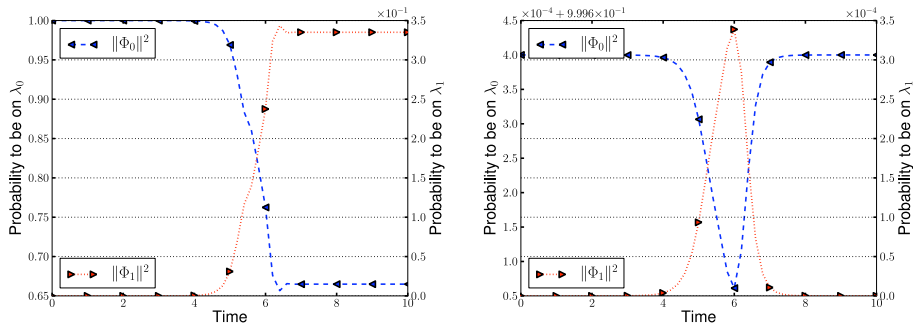


Figure 6: Time evolution of the probability of being in one of the adiabatic components (left $\delta = \epsilon = 0.2$, right $\delta = 5\epsilon = 1$). The left scale refers to the component $\Phi_{\mathcal{A}}$ (dashed line) on the upper level $\lambda_0 = E_{\mathcal{A}}(\cdot, \delta)$, while the right scale refers to the component $\Phi_{\mathcal{B}}$ (dotted line) on the lower level $\lambda_1 = E_{\mathcal{B}}(\cdot, \delta)$.

cases when the transition is significant makes the picture of the evolution of the energy interesting. See Figure 8. In the probability density and energy plots, dashed lines refer to the adiabatic component corresponding to $\lambda_0 = E_{\mathcal{A}}(\cdot, \delta)$. The dotted lines refer to the adiabatic component corresponding to $\lambda_1 = E_{\mathcal{B}}(\cdot, \delta)$. The solid lines refer to the whole wave function. The curves for the kinetic energy of the $\Phi_{\mathcal{A}}$ -part and $\Phi_{\mathcal{B}}$ -part in the left part of Figure 8 suggest a significant difference in momentum between them, and hence the opportunity for spawning a new family of semiclassical wavepackets. Note that the total norm and the energy of the numerical solutions in all cases are well conserved, even if larger wiggling appears for smaller gaps near the avoided crossing. This also happens in the corresponding simulations based on the Fourier discretization. Finally, in Figure 9 we plot the error in the adiabatic components and the error in the transition probability, when we consider as the exact solution the numerical solution provided by the Fourier method with $2^{12} = 4096$ points and Strang splitting with time-step $\tau = 0.02$. We note that we obtained very similar results when the initial wavepacket was associated with the lower energy level $E_{\mathcal{B}}$, which also guides the propagation scheme.

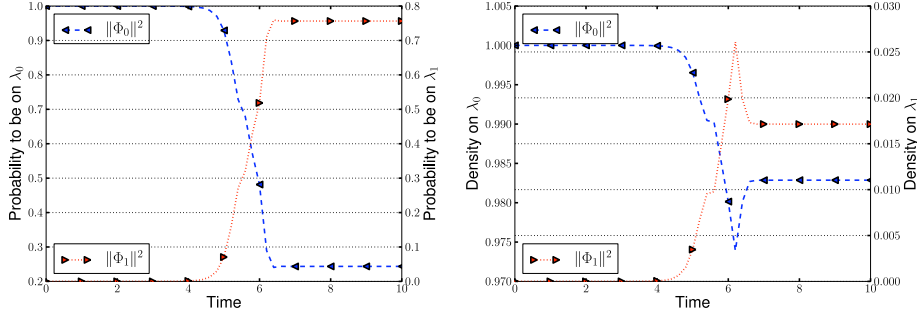


Figure 7: Time evolution of the probability of being in one of the adiabatic components (left $\delta = 0.5\epsilon = 0.1$, right $\delta = 2\epsilon = 0.4$). The left scale refers to the component $\Phi_{\mathcal{A}}$ (dashed line) on the upper level $\lambda_0 = E_{\mathcal{A}}(\cdot, \delta)$, while the right scale refers to the component $\Phi_{\mathcal{B}}$ (dotted line) on the lower level $\lambda_1 = E_{\mathcal{B}}(\cdot, \delta)$.

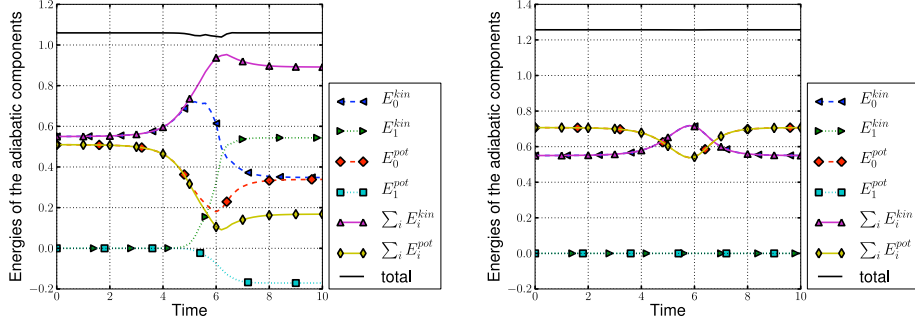


Figure 8: Energy evolution, left $\delta = \epsilon = 0.2$, right $\delta = 5\epsilon = 1$. Dashed lines refer to the adiabatic component corresponding to $\lambda_0 = E_{\mathcal{A}}(\cdot, \delta)$, dotted lines refer to the adiabatic component corresponding to $\lambda_1 = E_{\mathcal{B}}(\cdot, \delta)$, while plain lines refer to the whole wave function.

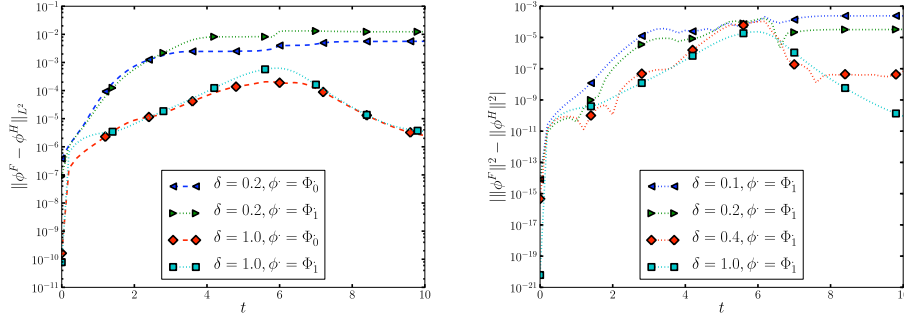


Figure 9: Time evolution of the error in the adiabatic components for $\epsilon = 0.2$ (left) and in the transition probability to the lower state (right). Dashed lines refer to the adiabatic component corresponding to $\lambda_0 = E_A(\cdot, \delta)$, while dotted lines refer to the adiabatic component corresponding to $\lambda_1 = E_B(\cdot, \delta)$.

References

- [1] V. BETZ AND B. GODDARD, *Accurate prediction of nonadiabatic transitions through avoided crossings*, Phys. Rev. Lett., 103 (2009), p. 213001.
- [2] V. BETZ, B. GODDARD, AND S. TEUFEL, *Superadiabatic transitions in quantum molecular dynamics*, Proc. Roy. Soc. A., Math., Phys., Eng. Science, 465 (2009), pp. 3553–3580.
- [3] E. FAOU, V. GRADINARU, AND C. LUBICH, *Computing semiclassical quantum dynamics with Hagedorn wavepackets*, SIAM J. Sci. Comput., 31 (2009), pp. 3027–3041.
- [4] V. GRADINARU, G. A. HAGEDORN, AND A. JOYE, *Tunneling dynamics and spawning with adaptive semi-classical wave-packets*, Journal of Chemical Physics, 132 (2010).
- [5] G. A. HAGEDORN, *Semiclassical quantum mechanics. I. The $\hbar \rightarrow 0$ limit for coherent states*, Comm. Math. Phys., 71 (1980), pp. 77–93.
- [6] G. A. HAGEDORN, *Semiclassical quantum mechanics. IV. Large order asymptotics and more general states in more than one dimension*, Ann. Inst. H. Poincaré Phys. Théor., 42 (1985), pp. 363–374.

- [7] G. A. HAGEDORN, *High order corrections to the time-dependent Born-Oppenheimer approximation II: Coulomb systems*, Commun. Math. Phys., 117 (1988), pp. 387–403.
- [8] —, *Molecular propagation through electron energy level crossings*, Memoirs, Amer. Math. Soc., 111 (536) (1994), pp. 1–130.
- [9] —, *Classification and normal forms for avoided crossings of quantum-mechanical energy levels*, J. Phys. A, 31 (1998), pp. 369–383.
- [10] G. A. HAGEDORN, *Raising and lowering operators for semiclassical wave packets.*, Ann. Phys., 269 (1998), pp. 77–104.
- [11] G. A. HAGEDORN AND A. JOYE, *Landau-Zener transitions through small electronic eigenvalue gaps in the Born-Oppenheimer approximation*, Ann. Inst. H. Poincaré Sect. A. Phys. Théor., 68 (1998), pp. 85–134.
- [12] G. A. HAGEDORN AND A. JOYE, *Determination of non-adiabatic scattering wave functions in a Born-Oppenheimer model*, Ann. Henri Poincaré, 6 (2005), pp. 937–990.
- [13] G. A. HAGEDORN AND A. JOYE, *Erratum to: “Determination of non-adiabatic scattering wave functions in a Born-Oppenheimer model” [Ann. Henri Poincaré 6 (2005), no. 5, 937–990; mr2219864]*, Ann. Henri Poincaré, 6 (2005), pp. 1197–1199.
- [14] M. KLEIN, A. MARTINEZ, R. SEILER, AND X. WANG, *On the Born-Oppenheimer expansion for polyatomic molecules*, Comm. Math. Phys., 143 (1992), pp. 607–639.
- [15] L. LANDAU, *Collected Papers of L. D. Landau, Edited and with an introduction by D. ter Haar*, New York, Gordon and Breach, 1967.
- [16] C. LASSER AND T. SWART, *Single switch surface hopping for a model of pyrazine*, The Journal of Chemical Physics, 129 (2008), p. 034302.
- [17] H. NAKAMURA, *Nonadiabatic transition : concepts, basic theories and applications*, New Jersey, N.J. : World Scientific, 2002.
- [18] —, *Advances in Chemical Physics*, vol. 138, John Wiley & Sons, Inc., 2008, ch. Nonadiabatic Chemical Dynamics: Comprehension and Control of Dynamics, and Manifestation of Molecular Functions.

- [19] S. NANBU, T. ISHIDA, AND H. NAKAMURA, *Future perspectives of nonadiabatic chemical dynamics*, Chem. Sci., 1 (2010), pp. 663–674.
- [20] P. PUZARI, S. DESHPANDE, AND S. ADHIKARI, *A quantum-classical treatment of non-adiabatic transitions*, Chemical Physics, 300 (2004), pp. 305 – 323.
- [21] V. ROUSSE, *Landau–Zener transitions for eigenvalue avoided crossings in the adiabatic and Born–Oppenheimer approximations*, Asympt. Anal., 37 (2004), pp. 293–328.
- [22] J. TULLY, *Molecular dynamics with electronic transitions*, The Journal of Chemical Physics, 93 (1990), p. 1061.
- [23] J. TULLY AND R. PRESTON, *Trajectory surface hopping approach to nonadiabatic molecular collisions: The reaction of H^+ with D_2* , J. Chem. Phys., 55 (1971), pp. 562–572.
- [24] C. ZENER, *Non-adiabatic crossing of energy levels*, Proc. Phil. Soc. London, 137 (1932), pp. 696–702.
- [25] A. ZEWEIL, *Femtochemistry: Ultrafast Dynamics of the Chemical Bond*, World Scientific, Singapore, 1994.

Research Reports

No.	Authors/Title
11-33	<i>R. Bourquin, V. Gradinaru and G.A. Hagedorn</i> Non-adiabatic transitions near avoided crossings: theory and numerics
11-32	<i>J. Šukys, S. Mishra and Ch. Schwab</i> Static load balancing for multi-level Monte Carlo finite volume solvers
11-31	<i>C.J. Gittelsohn, J. Könnö, Ch. Schwab and R. Stenberg</i> The multi-level Monte Carlo Finite Element Method for a stochastic Brinkman problem
11-30	<i>A. Barth, A. Lang and Ch. Schwab</i> Multi-level Monte Carlo Finite Element method for parabolic stochastic partial differential equations
11-29	<i>M. Hansen and Ch. Schwab</i> Analytic regularity and nonlinear approximation of a class of parametric semilinear elliptic PDEs
11-28	<i>R. Hiptmair and S. Mao</i> Stable multilevel splittings of boundary edge element spaces
11-27	<i>Ph. Grohs</i> Shearlets and microlocal analysis
11-26	<i>H. Kumar</i> Implicit-explicit Runge-Kutta methods for the two-fluid MHD equations
11-25	<i>H. Papasaïka, E. Kokioïpoulou, E. Baltasavias, K. Schindler and D. Kressner</i> Sparsity-seeking fusion of digital elevation models
11-24	<i>H. Harbrecht and J. Li</i> A fast deterministic method for stochastic elliptic interface problems based on low-rank approximation
11-23	<i>P. Corti and S. Mishra</i> Stable finite difference schemes for the magnetic induction equation with Hall effect
11-22	<i>H. Kumar and S. Mishra</i> Entropy stable numerical schemes for two-fluid MHD equations
11-21	<i>H. Heumann, R. Hiptmair, K. Li and J. Xu</i> Semi-Lagrangian methods for advection of differential forms
11-20	<i>A. Moïola</i> Plane wave approximation in linear elasticity